Chapter 2
Viscosity and Normal Stress Differences

Abstract Viscosity is the property most used with molten plastics. It relates the shear stress to the shear rate in steady simple shear flow, which is the deformation generated between two parallel plates, one of which undergoes linear displacement. For viscoelastic fluids, two other quantities are needed for a complete description of the stress field, and these are the *first and second normal stress differences*. The viscosity and the two normal stress differences are functions of shear rate that are called the *viscometric functions*, and flows governed by these are called *viscometric flows*. In addition to simple shear, other viscometric flows include flow in straight channels and rotational flows between concentric cylinders, between a cone and plate and between two disks. Flow in an extruder is dominated by the viscometric functions, mainly the viscosity. This chapter describes the dependence of viscosity on shear rate, temperature, molecular weight and its distribution, tacticity, comonomer content, and long-chain branching.

2.1 Simple Shear and Steady Simple Shear

Simple shear is of central importance in applied rheology for two reasons. First, it is the flow that is the easiest to generate in the laboratory, and melt data most often reported are based on flows that are rheologically equivalent to simple shear. Secondly, a number of processes of industrial importance, particularly extrusion and flow in many types of die, approximate steady simple shear flow. Finally, the flow behavior of melts in these flows is governed mainly by viscosity, and elasticity is not an important factor. It is thus appropriate to devote a chapter to the properties that govern simple shear flow.

Simple shear was introduced in Sect. 1.4.2, and we will review its essential features here. Referring to Fig. 2.1, we show this flow being generated by the rectilinear motion of one flat plate relative to another, where the two plates are parallel and the gap between them h is constant with time. This flow is completely

J. M. Dealy and J. Wang, *Melt Rheology and its Applications in the Plastics Industry*, Engineering Materials and Processes, DOI: 10.1007/978-94-007-6395-1_2,

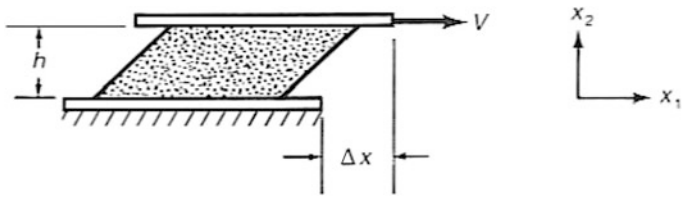

Fig. 2.1 Simple shear flow in x_1 direction

described by giving the shear strain γ as a function of time, where γ was defined by Eq. (1.8), which is repeated below as (2.1). The shear rate $\dot{\gamma}$ is the derivative of this quantity with respect to time and is thus the velocity of the moving plate divided by the gap, as was shown by Eq. (1.9), repeated below as (2.2). In *steady simple shear* the shear rate is constant with time.

$$\gamma = \Delta X/h \tag{2.1}$$

$$\dot{\gamma} = \frac{1}{h}\frac{\mathrm{d}X}{\mathrm{d}t} = \frac{V}{h} \tag{2.2}$$

According to a universally used convention, the velocity components in simple shear are defined as follows in terms of the coordinate system shown in the Fig. 2.1.

V is the velocity of the upper plate.
v_1 is the velocity of the fluid in the x_1 direction.
The velocities in the x_2 and x_3 directions are zero.
The velocity gradient is in the x_2 direction.

Simple shear is a uniform deformation, i.e., each fluid element undergoes the same deformation, and the strain and strain rate are independent of position in space; and for steady simple shear the strain rate is constant with time. Thus, the strain rate of every fluid element is the same and given by:

$$\dot{\gamma} = \mathrm{d}v_1/\mathrm{d}x_2$$

As a result, the rheologically meaningful stresses are also independent of position in space.

2.2 Viscometric Flow

We will define a viscometric flow as one that, from the point of view of a fluid element, is indistinguishable from steady simple shear. A more comprehensive mathematical definition can be found in the book by Bird et al. [1]. Thus, while various fluid elements in the field of flow may be subject to different shear rates,

the shear rate experienced by any particular fluid element is constant with time. Steady simple shear is the simplest possible viscometric flow.

Viscometric flows are of practical interest, not only because of their wide use in experimental rheology, but also because many flows of practical importance are viscometric flows or close approximations thereto. Some examples are listed below:

1. Steady tube flow (Poiseuille flow)

This flow is the one most often used to determine the viscosity of molten plastics. It also occurs whenever a melt is transported by means of circular channel. The magnitudes of the shear stress and shear rate vary from zero on the axis to a maximum at the wall.

2. Steady slit flow

Sometimes called plane Poiseuille flow, slit flow can also be used to measure viscosity. The shear stress and shear rate vary from zero on the plane of symmetry to a maximum at the walls.

3. Annular pressure flow

This flow occurs in the axial direction in the space between two concentric cylinders as the result of a pressure gradient. If the ratio of the two diameters is close to one, the velocity distribution approaches that for slit flow.

4. Steady concentric cylinder (Couette) Flow

This is a *drag flow* generated by the rotation of either the inner or outer cylinder of a concentric cylinder apparatus. It is widely used for the measurement of viscosity in Newtonian fluids, but is not convenient for use with melts. If the ratio of the two diameters is close to one, the shear rate becomes nearly uniform in the annular gap containing the fluid and thus approximates that in steady simple shear flow.

5. Steady parallel disk flow

This involves torsional flow of fluid between two parallel discs generated by the rotation of one of the disks. Also called plate–plate flow

6. Steady cone and plate flow

This flow is approximately viscometric and is of special interest, because if the cone angle is very small, the shear rate and shear stress are very nearly uniform, and the viscosity and first normal stress difference can be readily measured. The use of this flow, however, is limited to quite low shear rates because of the substantial departures from viscometric flow that occur at higher rates.

7. Steady sliding cylinder flow

This is a drag flow of fluid between concentric cylinders generated by the linear displacement of the inner cylinder. If the ratio of the diameters of the two cylinders is close to one, the shear rate is nearly uniform in the gap.

8. Steady helical flow

This is a combination of flows 4 and 7. The fluid is contained in the annular space between two concentric cylinders; one of these rotates at a constant speed while either the same or the other cylinder is displaced along its own axis at a constant speed.

9. Combined drag and pressure flow

If we combine steady simple shear with pressure flow in a slit, there are two forces driving fluid flow. Drag flow results from the motion of one wall, while pressure flow results from the pressure gradient. If the direction of the pressure gradient is the same as the direction of the motion of the moving wall, the velocity profile is of one of the types shown in Fig. 2.2 [1]. Depending on the sign of the pressure gradient, pressure can work with or against the drag flow, and four situations are illustrated in the figure. Note that a negative pressure gradient ($dp/dx < 0$) promotes flow from left to right, while a positive gradient works against the drag flow. If the direction of the drag flow is at an angle to the direction of the pressure gradient, the resulting deformation is similar to that in the channel of a single screw extruder. A similar combined flow is Couette (concentric cylinder) flow with an axial pressure gradient. Here the drag flow is perpendicular to the pressure flow direction. When the gap is very small, this flow becomes equivalent to plane Couette flow with perpendicular pressure flow.

All of the analyses presented or cited above are based on the *no-slip* assumption that the fluid adheres to any wall with which it is in contact and that if this wall moves, the fluid in contact with it moves at the same speed. However, this assumption is not always valid for molten plastics. For certain combinations of shear stress and shear strain, the melt undergoes some type of fracture at or near the wall and subsequently undergoes slip. In the case of linear polyethylene this occurs at shear stresses in the neighborhood of 0.1 MPa unless the experiment is terminated while the total shear strain is still quite small. Once slip flow begins, the velocity of the sliding polymer surface relative to the wall is not known a priori. This complicates the interpretation of data to determine the viscometric functions. Wall slip is discussed in further detail in Chap. 6.

Another assumption that is made in the classical analyses of viscometric flows is that the deformation is homogeneous. In reality, an experimental apparatus is

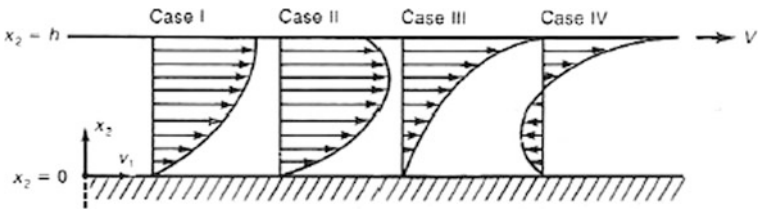

Fig. 2.2 Velocity profiles for combined drag and pressure flows. Cases I and II: $dp/dx < 0$; Cases III and IV: $dp/dx > 0$. Adapted from Ref. [1]

always finite in size, and the sample has one or more exposed free surfaces. Examples are the sample edge in a cone and plate or parallel disk rheometer. In addition, there may be zones in the field of flow where the deformation differs significantly from the assumed viscometric flow. Examples are the zones below the inner cylinder of a Couette viscometer and at the entrance of a capillary rheometer. These end and edge effects can be sources of error in viscometric measurements and are considered in some detail in Chap. 6.

2.3 The Viscometric Functions

As was pointed out in Chap. 1, for an incompressible material a normal stress by itself has no rheological significance, since if the normal stresses are the same in all directions, i.e. the stress is isotropic, there will be no deformation. Only normal stress differences can cause deformation, for example stretching and compression. There are two, independent, normal stress differences, and these are called the *first and second normal stress differences*. These, along with the viscosity, are functions of shear rate, and are called the *viscometric functions*.

$$\eta(\dot{\gamma}) \equiv \sigma/\dot{\gamma} \tag{2.3}$$

$$N_1(\dot{\gamma}) \equiv \sigma_{11} - \sigma_{22} \tag{2.4}$$

$$N_2(\dot{\gamma}) \equiv \sigma_{22} - \sigma_{33} \tag{2.5}$$

For any viscometric flow, the three viscometric functions completely describe the rheological behavior of a fluid. In other words, these constitute all the rheological information that can be obtained from measuring the stress components.

2.4 The Viscosity

Viscosity is the rheological property most often used to characterize molten plastics, because it is relatively easy to measure, provides some information about molecular structure, and plays an important role in melt processing. Like all rheological properties the viscosity (and normal stress differences) of a polymer depend on the following factors:

1. Flow conditions

   (a) Shear rate
   (b) Temperature
   (c) Pressure

2. Resin composition and molecular structure
   (a) Chemical nature of polymer
   (b) Molecular weight distribution
   (c) Presence of long chain branches
   (d) Nature and concentration of additives, fillers, etc.

The viscosity at high shear rates is determined by use of a capillary rheometer, while that at low rates it is measured using a rotational rheometer with cone-plate fixtures. The actual range of shear rates accessible using either instrument depends on the properties of the melt, as is explained in Chap. 6. These instruments are able to generate the steady shear flow that is required to measure viscosity. The entire viscosity curve is rarely used for routine quality control. The device most used for this application is the *melt indexer*, more properly called an *extrusion plastometer*. While this very simple flow tester involves flow through a short capillary, it does not provide a reliable value of viscosity. Experimental methods are described in detail in Chap. 6.

2.4.1 Effect of Shear Rate on Viscosity

As in the case of Newtonian fluids, the viscosity of a polymer depends on temperature and pressure, but for polymeric fluids it also depends on shear rate, and this dependency is quite sensitive to molecular structure. In particular, comprehensive and precise data of viscosity versus shear rate can be used to infer the molecular weight distribution of a linear polymer. And it can sometimes tell us something about the level of long-chain branching. This curve is also of central importance in plastics processing, where it is directly related to the torque and energy required to extrude a melt and is useful in the design of extruders and dies.

The viscosity of molten thermoplastics decreases sharply as the shear rate increases. Typical behavior is sketched in Fig. 2.3. Note that linear rather than logarithmic scales are used here. At very low shear rates, the viscosity normally becomes independent of shear rate, as shown in the magnified inset of Fig. 2.3. The constant viscosity that prevails at these low shear rates is called the *zero-shear viscosity* and has the symbol η_0. The zero shear viscosity is an important scaling parameter, as is shown below, but for many commercial resins, particularly those with very broad molecular weight distributions or a high degree of long chain branching, it is difficult to measure using controlled strain rotational rheometers. This is because the shear rate at which $\eta(\dot{\gamma})$ levels out to its limiting value is too low to be generated in these instruments. It is often necessary to resort to a long-duration creep experiment to determine η_0. More will be said about this in Chap. 6.

In order to show clearly the approach of the viscosity to its limiting, low shear-rate value, while also showing high shear-rate behavior, it is customary to display viscosity versus shear rate behavior as a plot of $\log(\eta)$ versus $\log(\dot{\gamma})$. An example of such a plot is shown in Fig. 2.4, which shows the data of Meissner [2] for a

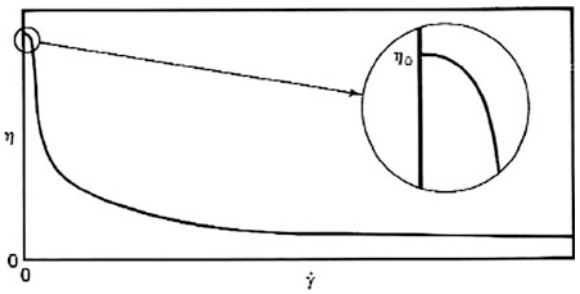

Fig. 2.3 Shape of viscosity versus shear rate curve for a molten polymer. Using linear scales important low shear rate features are crowded into the left-hand axis. The inset is an expansion of this region

low-density polyethylene at several temperatures. This polymer has a broad molecular weight distribution and a high level of long-chain branching. As a result the decrease in viscosity from its zero-shear value to a power-law region extends over many decades of shear rate. To obtain the data at very low shear rates, it was necessary to make major modifications to a commercial rotational rheometer, and the measurements required great skill and very long measurement times. At the lowest shear rates we see a clearly-defined "Newtonian" region over which the viscosity is constant. And at the highest shear rates, the curves tend to approach each other, appearing to move onto straight lines, suggesting power-law behavior.

For linear polymers with narrow molecular weight distributions, the viscosity curve (on a log–log plot) has a distinct region of essentially constant viscosity as well as a well-defined power law region, and the transition between the two occurs over about one decade of shear rate. This is illustrated in Fig. 2.5, where data for several, narrow molecular weight distribution polystyrenes are shown [3]. For these specially-polymerized samples the range of shear rates between the low-rate Newtonian region and a well-defined power law is much narrower than in the case of the LDPE data shown in Fig. 2.4. Also, we see that the curves for samples with

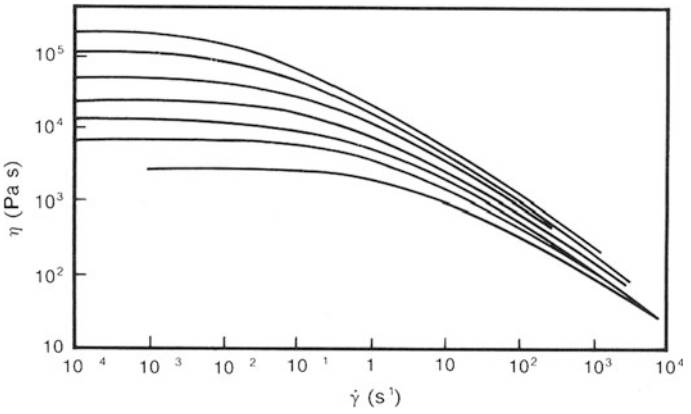

Fig. 2.4 Viscosity versus shear rate of a LDPE at several temperatures; from *top* to *bottom*: $T(°C) = 115, 130, 150, 170, 190, 210$, and 240. Data of Meissner [2]

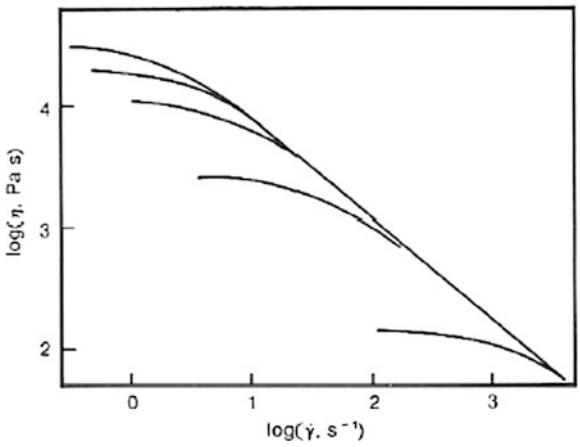

Fig. 2.5 Viscosity versus shear rate for narrow MWD polystyrenes; from *top to bottom* $M_w = 4.9 \times 10^4$, 12×10^4, 18×10^4, 22×10^4, and 24×10^4. From Stratton [3]

various molecular weights converge onto a single power-law line at shear rates that decrease with molecular weight. This power law is described by Eq. (2.6).

$$\sigma = k\dot{\gamma}^n \tag{2.6}$$

In terms of viscosity this becomes Eq. (2.7).

$$\eta = k(\dot{\gamma})^{n-1} \tag{2.7}$$

Obviously, a Newtonian fluid is a special case for which $n = 1$ and K is equal to the viscosity.

There are several undesirable features of the power law expressed by Eqs. (2.6) and (2.7).

1. The units of K depend on the value of n, and unless n is unity, they involve time to a power that is not an integer.
2. If the shear rate is negative, the equation does not yield a value for the viscosity (unless n is an integer).
3. The zero shear viscosity does not appear as a parameter.
4. The equation is only valid at high shear rates.

The first three undesired features can be eliminated by use of the following form:

$$\eta = \eta_0|\lambda\dot{\gamma}|^{n-1} \tag{2.8}$$

where λ is a material constant with units of time, i.e., a characteristic time of the material. Specifically, it is the reciprocal of the shear rate at which η becomes equal to η_0. A variation of (2.8) that is occasionally used is:

$$\eta = \eta_1|\dot{\gamma}|^{n-1}$$

where η_1 is numerically equal to the viscosity at a shear rate of 1 s^{-1}.

While Eq. (2.8) still cannot describe the low-shear-rate portion of the curve, where the viscosity approaches a constant value, for many polymers Eq. (2.6) [and Eqs. (2.7) or (2.8)] holds reasonably well over the high-shear-rate range of interest for processing. It has been widely used in the modeling of melt flow because of its mathematical simplicity, and this makes it possible to derive analytical expressions describing flows in extruders and channels. However, because of the wide availability of powerful computational facilities, the power law no longer offers an important advantage, and more realistic equations are now being used in most process simulations. These allow for the transition to Newtonian behavior over a range of shear rates.

As suggested by Eq. (2.8), the variation of η with $\dot{\gamma}$ implies the existence of at least one material property with units of time, and in that model this parameter, λ, is the reciprocal of the shear rate at which the power-law line reaches η_0. Models that can describe the approach to η_0 thus involve at lease one characteristic time. Examples of modified power laws whose parameters are η_0, a characteristic time, and an exponent, include the Cross equation [4] and the Carreau equation [5], shown below as Eqs. (2.9) and (2.10) respectively.

$$\eta(\dot{\gamma}) = \eta_0[1 + (\lambda|\dot{\gamma}|)^m]^{-1} \tag{2.9}$$

$$\eta(\dot{\gamma}) = \eta_0\left[1 + (\lambda\dot{\gamma})^2\right]^{-p} \tag{2.10}$$

These models approach power-law behavior at high shear rates, and the dimensionless material constants m and p are simply related to the power law exponent, i.e., $m = 1-n$ and $p = (1-n)/2$. Hieber and Chiang [6] compared the ability of these two models to fit data for a variety of commercial polymers for purposes of flow simulation. They found that the Cross equation provided a better fit for the polymers they considered.

For more flexibility in fitting data, Yasuda et al. [7] generalized Eq. (2.10) by adding an additional parameter as shown in Eq. (2.11) in order to adjust the curvature in the transition region.

$$\eta(\dot{\gamma}) = \eta_0[1 + (\lambda\dot{\gamma})^a]^{(n-1)/a} \tag{2.11}$$

This is often called the Carreau-Yasuda equation.

Elberli and Shaw [8] reported that time constants obtained by fitting data to two-parameter viscosity models were less sensitive to experimental error than those based on models with more parameters. Data at low shear rates and around the reciprocal of the time constant are most essential to obtain useful values of the parameters, while the high shear rate data are less important.

Plumley [9] evaluated the ability of the above models to fit data for linear and sparsely-branched metallocene polyethylenes. They found that the Cross equation gave a good fit to the data and that adding parameters did not lead to a significant improvement. On the other hand, for a linear polymer with a bimodal molecular weight distribution or polymers with long-chain branching, such as LDPE, three-

parameter models are not able to fit data over a very broad range of frequencies. Wang [10] proposed a "double-Cross" model to describe the behavior of such materials. It is the sum of two Cross model terms (Eq. 2.9), each with its own set of three parameters. Wang found that this model could fit both the low-shear-rate approach to the zero-shear viscosity as well as the high-shear-rate approach to a power law with great precision.

Equations such as those presented above are sometimes used to extrapolate low-shear-rate data to estimate the zero-shear viscosity when data do not reach the Newtonian region. But this is not a reliable procedure, since there is no theoretical basis for it, and it can yield values that are 50 % or more away from the correct value.

In Chap. 7 we will see that the molecular weight distribution of a linear polymer can be inferred from viscosity data obtained over a broad range of shear rates.

2.4.2 The Cox-Merz "Rule"

In Chap. 3 it is shown that small amplitude oscillatory shear using a rotational rheometer is the most widely used technique for the determination of linear viscoelastic properties. Using a small sample and a single instrument, it is possible to obtain data over a wide range of frequencies. One way of presenting the resulting data is a plot of magnitude of the complex viscosity $|\eta^*(\omega)|$ versus frequency. This is often referred to simply as the "complex viscosity" or the "dynamic viscosity." This is much less trouble than measuring the viscosity over a wide range of shear rates using at least two rheometers. It would thus be useful to be able to relate the complex viscosity to the (steady-shear) viscosity. Based on data for two polystyrenes, Cox and Merz [11] reported that the curve of *apparent viscosity* versus shear rate measured using a capillary viscometer was very similar to the curve of complex viscosity versus frequency. We will see in Chap. 6 that the apparent viscosity calculated from capillary viscometer data, i.e., the wall shear stress divided by the apparent shear rate, is substantially different from the actual viscosity, but it is possible that for the two polymers Cox and Merz studied the apparent viscosity was closer to the true value than is generally the case. What they observed was that the curve traced by their $\eta_A(\dot{\gamma}_A)$ data was very similar to that traced by $|\eta^*(\omega)|$ data. If the two curves were in fact identical, it would imply that:

$$\eta_A \equiv \frac{\sigma_w}{\dot{\gamma}_A} \cong |\eta^*|(\omega) \quad \text{with } \dot{\gamma}_A = \omega. \tag{2.12}$$

Over time, however, these details have been forgotten, and one refers now to a "Cox-Merz rule" which is expressed by Eq. (2.13).

$$\eta(\dot{\gamma} = \omega) = |\eta^*|(\omega) \tag{2.13}$$

Thus, the original observation, based on the apparent viscosity, has come to be replaced by a quantitative relationship. However, it has often been reported that

the relationship expressed by Eq. (2.13) is obeyed by experimental data, although this conclusion is sometimes based on the use of a small log–log graph on which significant deviations can easily hide. The Cox-Merz rule has been examined critically by Utracki and Gendron [12] and by Venkatraman et al. [13]. The latter authors reported that Eq. (2.13) works fairly well for LDPE, but not for HDPE. In any event, we will see below that many viscosity-structure relationships originally developed for use with viscosity data are now often applied to complex viscosity data. One can look at this in two ways. On the one hand, it is simply an application of Eq. (2.13). Or, on the other hand, one can say that the relationship itself applies to the complex viscosity.

2.4.3 *Effect of Temperature on Viscosity*

In Chap. 3, the procedure called time–temperature superposition is explained in detail. Here we make use of this technique to show how the shear rate range over which viscosity information can be obtained can be extended beyond the range actually accessible using a given viscometer. The procedure is based on the idea that increasing temperature has an equivalent effect on viscosity as decreasing shear rate. This trend can be seen by inspection of Fig. 2.4, noting that increasing the temperature moves data to lower curves. If this effect is quantitatively the same at all shear rates, this implies that a single *horizontal shift factor* can be used to shift data on a log–log plot taken at several temperatures along the shear rate axis to coincide with those measured at a *reference temperature* T_0. This idea is expressed by Eq. (2.14). As explained in Sect. 3.12, for greater precision, a second shift factor, $b_T(T)$, normally equal to $(T_0\rho_0/T\rho)$, should also be applied to the viscosity, but it is usually close to unity and is often neglected.

$$\eta(\dot{\gamma}, T_0) = [1/\alpha_T(T)]\eta(\dot{\gamma} a_T, T) \tag{2.14}$$

Such a representation is called a *master curve* and is a plot of *reduced viscosity* $\eta(T)/a_T(T)$ versus reduced shear rate $\dot{\gamma} a_T(T)$. Note that the horizontal shift factor $a_T(T)$ is applied to both axes, because the definition of the viscosity involves the shear rate. By use of this procedure, the range of reduced shear rate range over which a master curve can be prepared is broader than the range of shear rates over which measurements can be made.

For a polymer well above its glass transition temperature, it is often found that the zero-shear viscosity obeys the well-known Arrhenius relationship shown by Eq. (2.15).

$$\eta_0(T) = \eta_0(T_0) \exp\left[\frac{E_a}{R}\left(\frac{1}{T} - \frac{1}{T_0}\right)\right] \tag{2.15}$$

The constant E_a is called the activation energy for flow. But this is the special case of Eq. (2.14) for shear rates where the viscosity equals η_0, which implies that the shift factor is give by Eq. (2.16).

$$a_T(T) = \frac{\eta_0(T)}{\eta_0(T_0)} = \exp\left[\frac{E_a}{R}\left(\frac{1}{T} - \frac{1}{T_0}\right)\right] \tag{2.16}$$

Since $\eta_0(T_0)$ is a constant for a given master curve, the shift factor is proportional to $\eta_0(T)$. Thus, a viscosity master curve can be prepared by plotting $\eta(T)/\eta_0(T)$ versus $\dot{\gamma}\eta_0(T)$.

It should be mentioned that time–temperature superposition is of limited utility with crystallizable polymers, because the range of temperatures over which measurements can be made is limited to that between the melting point and the temperature at which the polymer starts to decompose.

Time–temperature superposition is not useful for long-chain branched systems, although such materials are sometimes characterized in terms of specially-defined activation energies. This subject is discussed in detail in Chap. 3.

2.4.4 *Effects of Pressure and Dissolved Gas on Viscosity*

Whereas increasing temperature decreases the viscosity of melts, increasing pressure increases it, because compression of the melt decreases free volume. Pressure shift factors can be used to generate master curves just as temperature shift factors are used in time–temperature superposition. The Barus equation is often found to describe the pressure dependence of viscosity. This is shown as Eq. (2.17).

$$\ln\left[\frac{\eta_0(P)}{\eta_0(P_0)}\right] = \beta(P - P_0) \tag{2.17}$$

This implies that the pressure shift factor a_P is given by:

$$\ln[a_P(P)] = \beta(P - P_0) \tag{2.18}$$

Figure 2.6 shows the effect of pressure on the viscosity of a high-density polyethylene at 180 °C, and Fig. 2.7 is a maser curve based on the same data [14]. The horizontal shift factor is $a'_P(P)$, the prime indicating that the vertical shift factor was neglected, i.e., set equal to unity. The Barus Eq. (2.18) was found to fit the entire viscosity curve very well with b_P set at unity. Increasing the pressure from atmospheric 0.1 to 69 MPa ($\approx$10,000 psi) increases the viscosity by a factor of about two.

The HDPE for which data are shown in Figs. 2.6 and 2.7 was saturated with carbon dioxide at several pressures, and viscosity data are shown in Fig. 2.8; the corresponding master curve is shown in Fig. 2.9. The horizontal shift factor $a_{P,C}$

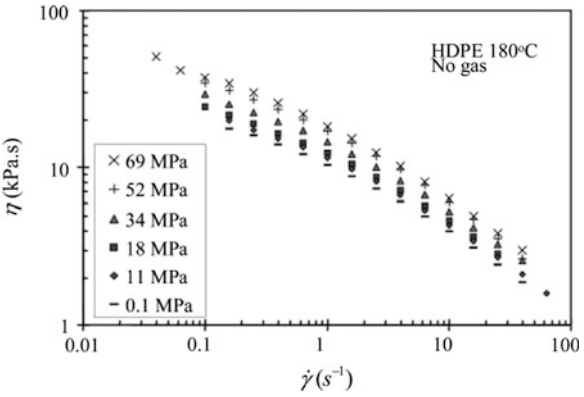

Fig. 2.6 Effect of pressure on the viscosity versus shear rate curve of HDPE. From Park and Dealy [14]

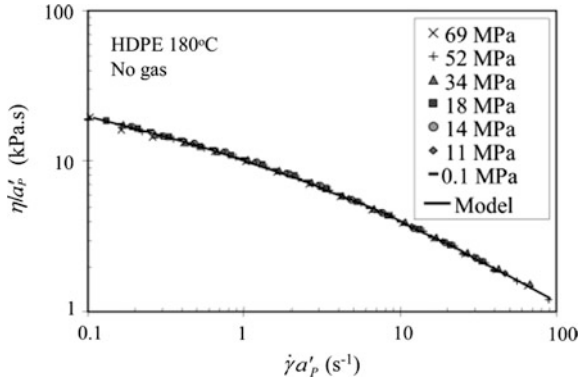

Fig. 2.7 Shifted viscosity curve taking b_P to be unity; reference pressure is 0.1 MPa. From Park and Dealy [14]

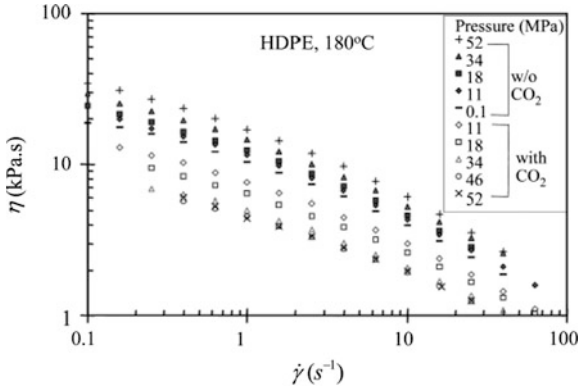

Fig. 2.8 Effects of pressure and dissolved CO_2 on viscosity. From Park and Dealy [14]

accounts for both pressure and gas concentration. The CO_2 reduced the viscosity by increasing free volume, thus counteracting the effect of pressure. The carbon dioxide not only neutralized the pressure effect but reduced the viscosity below its value at atmospheric pressure. At 69 MPa the viscosity is reduced by a factor of

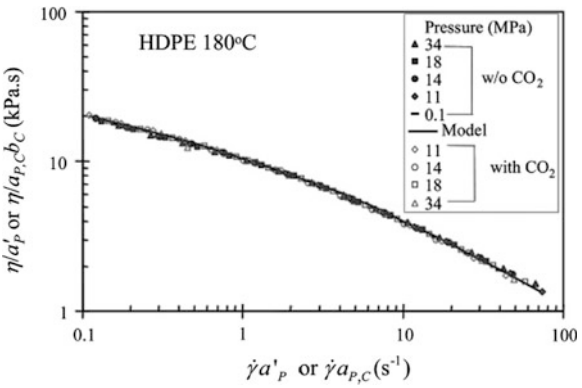

Fig. 2.9 Data of Fig. 2.8 shifted vertically and horizontally to make pressure-composition master curve. Vertical shift factor takes into account effect of concentration but not pressure. From Park and Dealy [14]

about 2.5. Park et al. [15] reported on the effect of long-chain branching on pressure shift factors for polystyrene and polyethylene.

2.4.5 *Effect of Molecular Weight on the Zero-Shear Viscosity*

Small molecules in the liquid state interact primarily through intermolecular forces that give rise at the microscopic level to friction and at the macroscopic level to viscosity. The viscosity of such a liquid is independent of shear rate. A polymeric liquid with a low molecular weight behaves in this way, and its viscosity increases linearly with molecular weight. For example, for linear polyethylene this behavior obtains up to a molecular weight around 3,500. But over a fairly narrow range of molecular weights the viscosity starts to decrease with shear rate and the increase of η_0 with molecular weight becomes much stronger than linear. In the same range of rates, the viscosity depends increasingly on shear rate.

Plots of $\log(\eta_0)$ versus $\log(M)$ for several linear, monodisperse polymers are shown in Fig. 2.10 [16]. At low molecular weights the viscosity is proportional to molecular weight and varies little with shear rate over a wide range of shear rates.

$$\eta \propto M \tag{2.19}$$

As the molecular weight increase, η_0 starts to increase much more rapidly with M, and the viscosity starts to depend strongly on shear rate. Over a fairly narrow range of M, data on a log–log plot approach a line with a slope between 3.4 and 3.6. In other words for linear, monodisperse polymers having sufficiently high molecular weight the relationship between $\log(\eta_0)$ and $\log(M)$ is given by Eq. (2.20).

$$\eta_0 = KM^{\alpha} \tag{2.20}$$

where α is usually the range of 3.5 ± 0.2

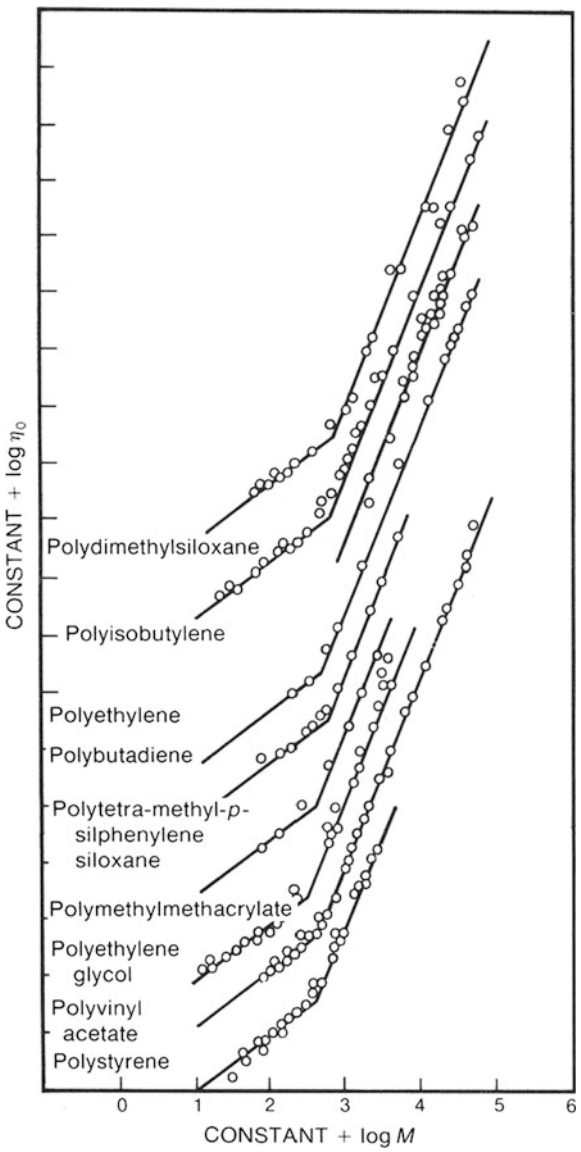

Fig. 2.10 Zero-shear viscosity versus molecular weight (logarithmic scales) for several polymers. The axes have been shifted to avoid crowding. The *low-MW lines* correspond to unentangled samples and have slopes of unity, while the *high-MW lines* correspond to entangled polymers and are fitted to lines having slopes of 3.4. From Berry and Fox [16]

The value of M where the lines described by Eqs. (2.19) and (2.20) intersect for a given polymer, M_C, is called the *critical molecular weight for entanglement*. Values of M_C for a number of polymers are given in Appendix A. This is not to be confused with two other rheologically meaningful critical molecular weights M'_C and M_e, which will be introduced later.

For polydisperse materials, it is found that Eq. (2.20) continues to be valid if M is simply replaced by the weight-average molecular weight, as long as there are very few unentangled molecules present, i.e. those with $M < M_C$.

$$\eta_0 = KM_w^{\alpha} \tag{2.21}$$

This relationship leads directly to a blending law for viscosity. For example, in a binary blend of two monodisperse samples of the same polymer having molecular weights M_1 and M_2, the weight-average molecular weight of the blend is given by:

$$M_{wb} = w_1 M_1 + w_2 M_2 \tag{2.22}$$

where w_1, and w_2, are the weight fractions of the blend components.

Using Eqs. (2.20) and (2.21) to eliminate the molecular weights, we have:

$$\eta_{0,b} = KM_w^{\alpha} = \left(w_1 \eta_{0,1}^{1/\alpha} + w_2 \eta_{0,2}^{1/\alpha}\right)^{\alpha} \tag{2.23}$$

This equation has been tested for blends of monodisperse [17, 18] and polydisperse [19] materials.

2.4.6 *Effect of Molecular Weight Distribution on Viscosity*

The effect of molecular weight distribution, MWD, is somewhat more subtle but still very important. In general, commercial polymers have a rather broad molecular weight distribution, although materials produced using metallocene catalysts can have polydispersities (M_w/M_n) as low as two. Figure 2.11 is a sketch of viscosity curves for two polymers having the same weight average molecular

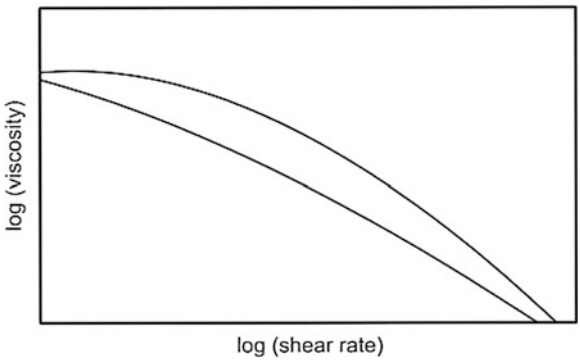

Fig. 2.11 Shapes of viscosity curves for two samples having the same M_w but with narrow (*upper curve*) and broad (*lower*) molecular weight distributions. The narrow MWD sample moves from a well-defined Newtonian region to power-law behavior over a narrower range of shear rates

weight but different molecular weight distributions. The upper curve is for a nearly monodisperse sample, while the lower one is for a sample with a moderately broad MWD. The broadening of the distribution stretches out the range of shear rates over which the transition from the zero-shear viscosity to the power law region occurs. Chapter 7 describes methods for using viscosity data to infer the MWD of a linear polymer, although it is to be noted that this requires data of high accuracy. In the plastics industry it is often desired to estimate polydispersity from easily measured quantities. Shroff and Mavridis [20] have compared several empirical correlations that have been proposed to do this.

2.4.7 *Effect of Tacticity on Viscosity*

The effect of tacticity on viscoelastic behavior is discussed in Chap. 3, but little has been published about its effect on viscosity. Fuchs et al. [21] studied a series of PMMAs that were 78 and 81 % syndiotactic as well as more conventional materials that were 59 % syndiotactic. They found that the zero-shear viscosities obeyed Eq. (2.20) with α equal to about 3.4. Figure 2.12 shows their results for two series of samples that were 59 and 81 % syndiotactic.

Figures 2.13 and 2.14 show data of Huang et al. [22] for iso-, stereo- and a tactic polystyrenes (iPS, sPS, aPS) having similar M_w values (about 2.5×10^5 g/mol) and polydispersities (2.3–2.5). The inset shows that dividing M_w by M_e made it possible to bring data for the three samples together on one line. M_e is the *molecular weight between entanglements* defined in Chap. 3. It is calculated from the plateau modulus and is one measure of the molecular weight at which

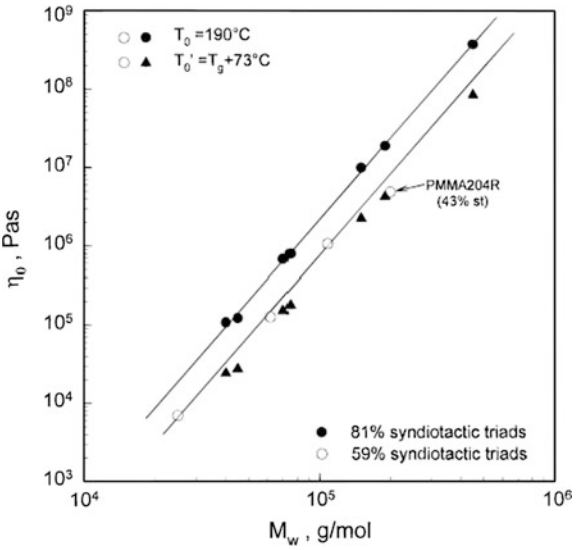

Fig. 2.12 Effect of tacticity on viscosity—Dependence of zero-shear viscosity at 190 °C on M_w for polypropylenes of varying tacticities. From Fuchs et al. [21]

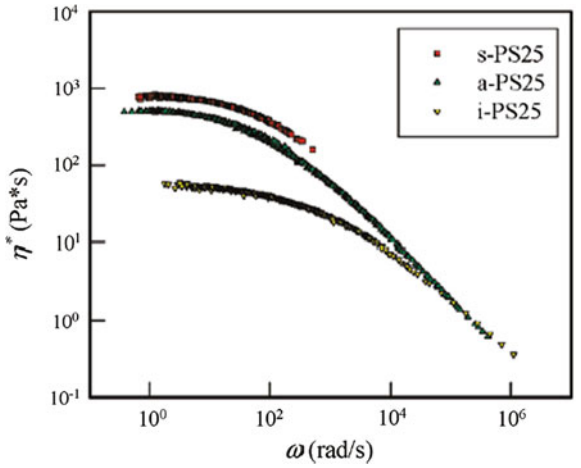

Fig. 2.13 Complex viscosity versus frequency of atactic, syndiotactic and isotactic polystyrenes at 280 °C. From Huang et al. [22]

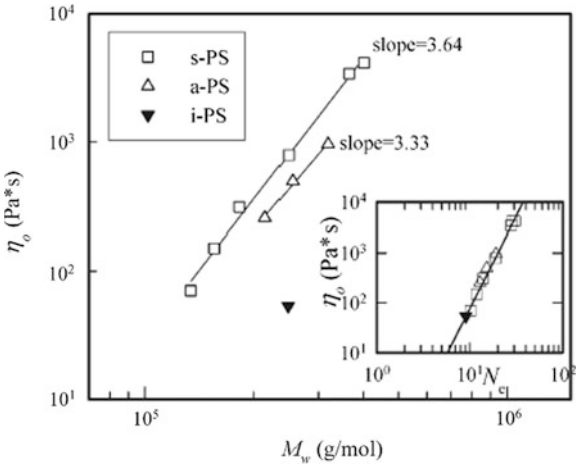

Fig. 2.14 Zero-shear viscosities of polystyrenes of Fig. 2.13 versus M_w. *The inset* shows viscosity versus "entanglement number" $N_e \equiv M_w/M_e$. From Huang et al. [22]

entanglement effects become prominent. The equation of the line in the inset of Fig. 2.14 is:

$$\eta_0 = 2.92 \times 10^{-2}(M_w/M_e)^{3.6} \tag{2.24}$$

2.4.8 Viscosity of Ethylene/Alpha-Olefin Copolymers

An important class of commercial polymers are copolymers of ethylene and an alpha-olefin, known as linear low density polyethylenes (LLDPE). The use of a

copolymer introduces short-chain side branches onto the polyethylene backbone, and the details of the molecular structure depend on the method of polymerization. If a heterogeneous, Ziegler catalyst is used, the side-chains tend to be distributed in blocks rather than randomly along the backbone. If the copolymer is prepared using a single-site (metallocene) catalyst, the short-chain branching distribution is expected to be random.

Wood-Adams et al. [23] studied the effect of comonomer content in three ethylene-butene copolymers prepared using a single-site catalyst, in which the butene level ranged from 11 to 21 %. While the three materials studied had polydispersities of about 2.0, there was a modest variation in average molecular weight, and this was accounted for by dividing the complex viscosity by the zero-shear viscosity. While the resulting master plots for the three materials were not precisely identical, the authors concluded that there was no significant effect of comonomer content on η_0. Wood-Adams and Costeux [24] found that the copolymers used in this study were thermorheologically simple, i.e., that they obeyed time–temperature superposition, and that the activation energy was insensitive to butene content at levels up to 7 wt %.

Garcia-Franco et al. [25] later studied this issue using a set of twelve ethylene/butene copolymers and also looked at data from several studies that involved other comonomers. They were able to correlate all their data using, in place of M_w, the average molecular weight per backbone bond m_b, and Fig. 2.15 shows their correlation. The line corresponds to Eq. (2.25), and while there is considerable scatter on this highly compressed log–log plot, a general trend is suggested.

$$\eta_0 = 4.73 \times 10^{-10} \left(\frac{M_w}{M_b}\right)^{3.33} \tag{2.25}$$

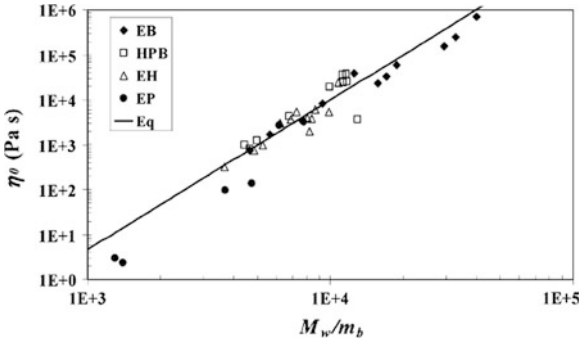

Fig. 2.15 Zero-shear viscosity at 190 °C for various polyolefins versus M_w/M_b, where M_b is the average molecular weight per backbone bond. *EB* Ethylene/butane copolymers; *EP* Ethylene/propylene; *EH* Ethylene/hexane; *HPB* Hydrogenated polybutadiene. From Garcia-Franco et al. [25]

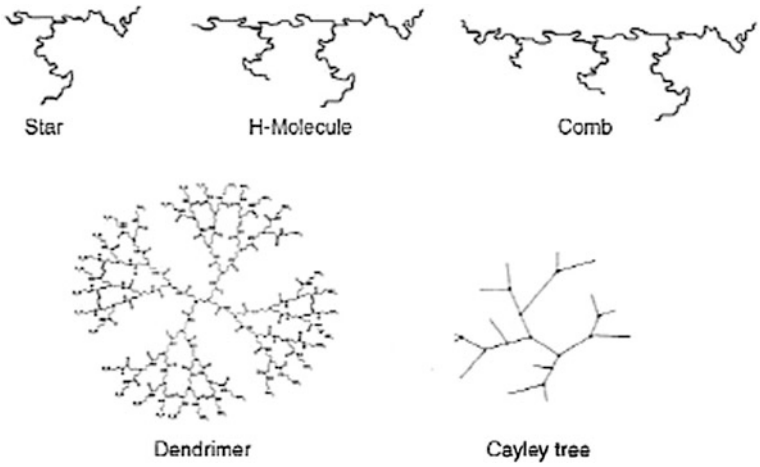

Fig. 2.16 Sketches of several branching structures: *star*, *H-shaped*, *comb*, *dendrimer* and *cayley tree* (branch-on-branch)

2.4.9 Effect of Long-Chain Branching on Viscosity

Branches are "long" from our point of view if they are sufficiently entangled to affect rheological behavior. For viscosity we might expect the molecular weight for the onset of branching effects to be M_C, which is about $3M_e$. The effect of branching also depends very much on the branching structure, i.e., lengths of branches, distance between branch points, and level of branching (branches on branches). Figure 2.16 shows several types of branching structure that will be referred to in the following discussion. It is not possible to infer branching structure from viscosity data unless something is known about the way a sample was polymerized. The effect of branching structure on rheological behavior is dealt with at length by Dealy and Larson [26]. Levels of long-chain branching too low to be detected using GPC can have a significant effect on viscosity, so rheology is a valuable tool for characterizing LCB.

To study the effects of specific types of LCB, it is necessary to work with polymers that have well-known branching structures. Small samples of such materials can be prepared by means of anionic polymerization, and this technique has been widely used in rheological studies. There is still a gap, however, between what is known about such materials and our understanding of structure-rheology relationships for highly-branched, commercial polymers.

2.4.9.1 Zero-Shear Viscosity of Monodisperse, Star-Shaped Polymers

For symmetric star polymers of a given molecular weight whose arms are too short to entangle, as the number of arms is increased η_0 falls progressively further below

that of a linear polymer with the same molecular weight. This is because the size of a molecule decreases as the number of branches increases at constant M. For a given number of arms, if the arm length is increased, η_0 rises above that of the linear polymer having the same M. When the arms become long enough to be well-entangled, however, i.e. when the arm molecular weight M_a reaches two or three times the molecular weight between entanglements M_e (defined in Chap. 3) η_0 increases approximately exponentially with molecular weight [27]. This phenomenon is illustrated in Fig. 2.17 which shows data of Kraus and Gruver [28] for linear, three-arm and four-arm polybutadiene stars. At moderate molecular weights the data for the stars lie below, but parallel to, the line for linear, entangled polymer with $\alpha = 3.4$, in accord with Eq. (2.20), but when the branch length reaches about $3M_e$ for three-armed stars, and about $4M_e$ for four-arm stars, the star data rise sharply and cross the line for linear polymers described by Eq. (2.20). Somewhat surprisingly, the viscosity of symmetric stars with entangled branches depends only on branch length and not on the polymer type or number of arms [27, 29], up at least 33 arms. The sharp increase in viscosity with M_a when arms are highly entangled is interpreted in terms of a molecular model in Chap. 4.

The picture is more complicated in the case of asymmetric stars. Gell et al. [30] studied a series of asymmetric stars made by adding arms of varying length at the midpoint of a very long backbone ($M/M_e \approx 40$). They found that even a short arm

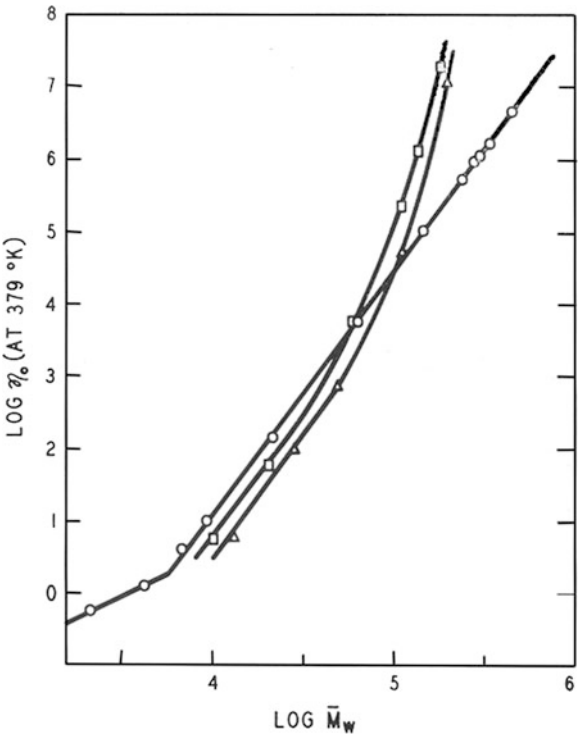

Fig. 2.17 Zero-shear viscosity at 379 °C versus M_w for polybutadienes having various structures: linear (*circles*), three-arm stars (*squares*), four-arm stars (*trangles*). At low Mw branched systems fall below the line for linear molecules, and at higher Mw their values rise above the line and approach an exponential behavior. From Kraus and Gruver [28]

with ($M_a/M_e = 0.5$ had the effect of tripling η_0, and for $M_a/M_e = 2.4$, η_0 was increased by a factor of ten. This illustrates the difficulty of inferring structural details from viscosity data unless one knows the type of structure present.

It is explained in Chap. 7 that the presence of chain segments with branch points at both ends, as in all the structures shown in Fig. 2.16 except the star, has a strong effect on extensional flow behavior.

While the use of specially synthesized polymers has advanced our knowledge of the effect of specific branching structures, relating rheological behavior to the structure of commercial branched polymers is a considerably more complex task. But the branching structure of commercial polymers is of great importance because of the very strong effect of certain branching structures on the processing behavior of thermoplastics.

2.4.9.2 Branched Metallocene Polymers

Polyolefins made using metallocene or related catalyst systems were the first commercial commodity polymers whose molecular structures were well-controlled and reproducible. It was thus possible to establish quantitative relationships between rheological behavior and structure. The linear homopolymers and ethylene-alpha-olefin copolymers have polydispersity indexes (M_w/M_n) very close to two. And *constrained geometry catalysts* [31, 32] can produce polymers with well-controlled, low levels of long-chain branching. These materials are sometimes said to be "substantially linear." Moreover, the branching structure of these polymers is well described by theory [33–37]. The first branches to be formed have one branch point, i.e., they are three-arm stars. As the branching level increases, molecules with two branch points start to appear; these are like the H-molecule shown in Fig. 2.16. A more detailed description of these polymers can be found in Sect. 7.2.3.

Wood-Adams et al. [23] reported the rheological properties of a series of polyethylenes made using such a catalyst. The branching levels were very low, ranging from 0.1 to 0.8 branches per 10,000 carbon atoms, and the polydispersities were very close to 2.0. The zero-shear viscosity increased very strongly with branching level, reaching nearly 70 times that of a linear polymer with the same molecular weight at the highest branching level, as shown in Fig. 2.18. Wood-Adams and Costeux [24] studied the effect of comonomer on branched polymers of this type. They found that all the long-chain branched polymers were thermorheologically complex, i.e., they did not obey time–temperature superposition, and that the activation energy based on the zero-shear viscosity was much higher for branched copolymers than for comparable branched homopolymers. The behavior of these samples is discussed in more detail in Chap. 7 where a technique is described for inferring the branching level in metallocene polymers from viscosity data.

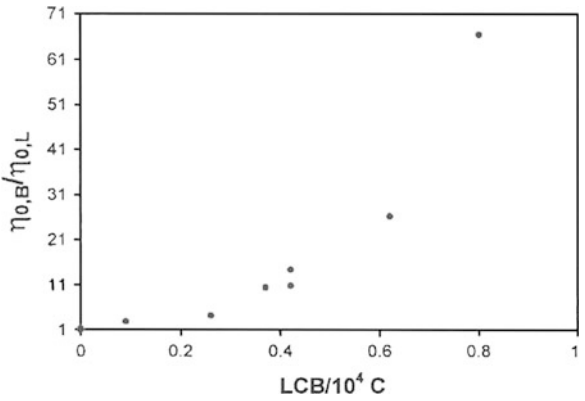

Fig. 2.18 Zero-shear viscosity of sparsely branched metallocene polyethylenes versus number of long-chain branches per 1,000 carbons. The viscosities are divided by that of linear PE having the same molecular weight. The first branched molecules to form at the *left* are stars, while as we move to the *right* there start to be H-molecules and very low levels of more highly-branched structures. From Wood-Adams et al. [23]

2.4.9.3 Viscosity of Randomly Branched Polymers and LDPE

We have already seen that the presence of long-chain branching, even at quite low levels, has a strong effect on the zero-shear viscosity and the shape of the viscosity curve. Random branching leads to a broad distribution of structures, making it difficult, if not impossible, to distinguish between the effects of branching and polydispersity. In fact, Wood-Adams and Dealy [38] demonstrated that one can, in principle, prescribe the molecular weight distribution of a linear polymer that would have the same complex viscosity as any given branched polymer. Low-density polyethylene is the commercial polyolefin with the most complex branching structure and poses the largest challenge in characterizing its structure. Laboratory studies of random branching usually make use of techniques in which increasing levels of branching are introduced into a linear precursor. While the results of these studies are instructive, their direct application to low-density polyethylene (LDPE) is limited.

Figure 2.19 shows complex viscosity as a function of frequency (similar to viscosity versus shear rate) for one linear and four branched ethylene/1-butene copolymers [39]. All five samples have nearly the same absolute molecular weight ($M_w \approx 155$ kg/mol), MWD ($M_w/M_n \approx 2$), and comonomer content. Sample A is linear, and the level of long-chain branching increases in the order B–C–D–E. We see that the zero-shear viscosity increases sharply with the level of branching but that all the data converge onto one curve at high shear rates.

Auhl et al. [40] studied the behavior of a series of polypropylenes that had been subjected to doses of electron beam radiation to generate various levels of long-chain branching. The ratio of the viscosity of a branched polymer η_0(br) to that of the linear precursor η_0(lin) is shown as a function of radiation dose d in Fig. 2.20. Assuming little chain scission, all these samples have the same molecular weight as

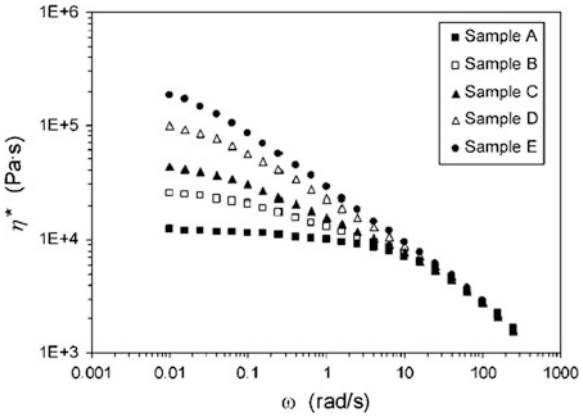

Fig. 2.19 Complex viscosity magnitude at 190 °C versus frequency for a linear (*Sample A*) and four branched polyethylene/1-butene copolymers. The branching level increases as we move through the alphabet. All samples have nearly the same absolute M_w (155 kg/mol) and polydispersity (2). Shear thinning begins at higher frequencies as we move from A to E, and at the highest frequencies all the curves come together. From Robertson et al. [39]

the linear precursor. Thus the point for $d = 0$ corresponds to $\eta_0(\text{br})/\eta_0(\text{lin}) = 1.0$. These data show the trend of increasing viscosity at low branching levels, reaching a peak and then decreasing. Comparing Figs. 2.18 and 2.20 makes it clear that the details of the branching structure have as important an effect on the zero-shear viscosity as the average degree of branching. The metallocene polyethylene (mPE)

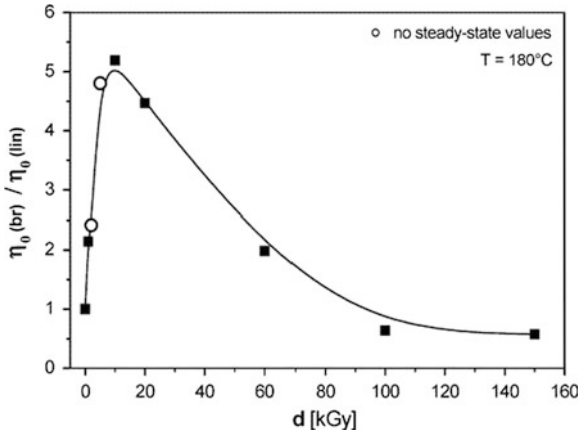

Fig. 2.20 Branching factor g, the ratio of η_0 of radiated polypropylene to that of linear PP precursor, versus radiation dose d. If little chain scission occurred all samples have the same molecular weight; i.e. $d = 0$ implies a branching factor of unity. Electron beam radiation has resulted in long-chain branching. The viscosity first increases sharply with branching level but then falls continuously to values below that of the linear precursor. From Auhl et al. [40]

(Fig. 2.18) always contains a large fraction of linear chains, and all the branch segments have the same size distribution as the linear chains. The irradiated polypropylene (PP) (Fig. 2.20), on the other hand, probably contains tree-like molecules with short branch segments. It is thus somewhat similar to a LDPE.

The most important commercial, branched polymer is low-density polyethylene (LDPE), which has a broad range of branching structures, with many short branches attached to tree- or comb-like molecules. In addition, LDPEs made in autoclaves have a distinctly different structure from those made in tubular reactors, as is explained in Chap. 7. All LDPEs are strongly shear-thinning, and we will see in Chap. 4 that they have a distinctive extensional flow behavior that is associated with high levels of long-chain branching.

The dependence of the zero-shear viscosity of LDPE [41–44] on average molecular weight is often compared with that of linear polymer having the same M_w, which is described by Eq. (2.20). However, two major questions arise in making such a comparison: obtaining a reliable value for η_0, and choosing an appropriate average molecular weight. Highly-branched, heterogeneous polymers such as LDPE have a very broad range of shear rates over which viscosity data make the transition from the Newtonian limiting value to a power-law region. It is generally not feasible to determine the zero-shear viscosity of LDPE using small-amplitude oscillatory shear, because the frequency required and the torque signal are extremely low. And extrapolation using an empirical viscosity model is highly unreliable. The LDPE viscosity data shown in Fig. 2.4 were obtained using a specially modified rotational rheometer, the operation of which required exceptional skill. The only reliable method is the long-time creep test described in Chap. 6. Such measurements can last several hours and require extra stabilization of the sample against thermo-oxidative degradation. Also, the activation energy defined by Eq. (2.30) has different values for linear PE and LDPE, so changing the temperature will alter the relationship between the viscosities of the two polymers.

The second issue regarding η_0 correlations for LDPE is the selection of a molecular weight average. Two averages have been used, one based on the size of molecules in solution, determined using GPC with universal calibration, and one based on mass, determined using light-scattering. Whichever one is selected, a collection of molecules having either similar sizes or similar masses will contain chains having a distribution of branching structures. Furthermore, LDPEs made in autoclaves have distinctly different branching structures than those made in tubular reactors. This issue is taken up in more detail in Sect. 7.2.5.

2.5 Normal Stress Differences

It was mentioned at the beginning of this chapter that there are two rheologically meaningful normal stress differences that can be measured in steady simple shear, the first and second normal stress differences. Based on the coordinate convention shown in Fig. 2.1, these are defined as:

$$N_1(\dot{\gamma}) \equiv \sigma_{11} - \sigma_{22} \tag{2.26}$$

$$N_2(\dot{\gamma}) \equiv \sigma_{22} - \sigma_{33} \tag{2.27}$$

These stress differences are associated with strain-induced anisotropy in a fluid, and in the case of polymeric liquids the anisotropy arises from the departure of molecules from their equilibrium, symmetrical average shape. In Chap. 8 we will find that the first normal stress difference is indirectly related to extrudate swell and that the second normal stress difference governs flow instabilities that occur in multi-layer profile coextrusion and flow through non-circular channels.

The first normal stress difference can be measured at low shear rates using a rotational rheometer equipped with cone-plate fixtures, although problems arise that are not encountered in the measurement of viscosity. The second normal stress difference is considerably more difficult to determine, and relatively few data have been reported. It has been observed that N_2 is negative with a magnitude about 1/3 that of N_1.

For a Newtonian fluid the shear stress is proportional to the shear rate, the normal stress differences are zero, and at sufficiently low shear rates viscoelastic materials approach Newtonian behavior. There are two simplified models that provide useful information about the first departures from Newtonian behavior as the shear rate is increased from zero. One of these is the second-order fluid model, and the other is the rubberlike-liquid model. Both of these models predict that the shear stress is still linear in shear rate (constant viscosity) but that the normal stress differences are quadratic in shear rate. This observation led to the definitions of the *first and second normal stress difference coefficients*, which these models predict are independent of shear rate.

$$\Psi_1(\dot{\gamma}) \equiv N_1(\dot{\gamma})/\dot{\gamma}^2 \tag{2.28}$$

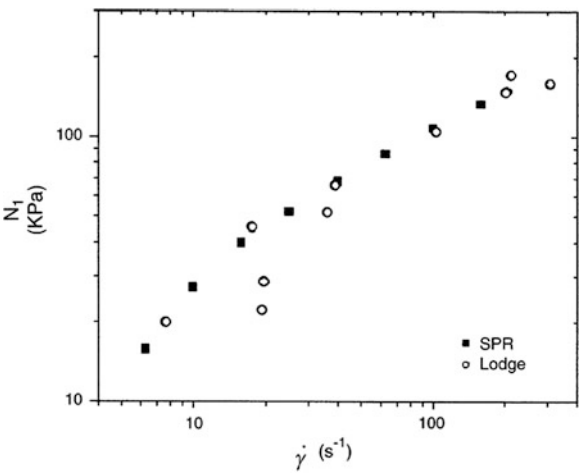

Fig. 2.21 First normal stress difference versus shear rate for a polystyrene measured using a Lodge stressmeter and a sliding plate rheometer (SPR). There is scatter in the stressmeter data around 20 s^{-1}, but most of the data show good agreement. From Xu et al. [48]

$$\Psi_2(\dot{\gamma}) \equiv N_2(\dot{\gamma})/\dot{\gamma}^2 \tag{2.29}$$

Data obtained at low shear rates have shown that Ψ_1 and Ψ_2 do indeed have limiting, non-zero values, which are assigned the symbols $\Psi_{1,0}$ and $\Psi_{2,0}$.

The second normal stress difference is usually reported in relation to the first normal stress difference by use of a shear-rate dependent normal stress ratio:

$$(\dot{\gamma}) \equiv \frac{-_2(\dot{\gamma})}{_1(\dot{\gamma})} = \frac{-N_2(\dot{\gamma})}{N_1(\dot{\gamma})} \tag{2.30}$$

This ratio has a non-zero limiting value as the shear rate approaches zero, and this value has been reported to be 0.24 for linear melts [45] and about 0.3 for stars [46].

As the shear rate increases, Ψ_1 decreases, but its value at high shear rates can not be determined using rotational rheometers due to flow disturbances. Data for a polybutadiene and a polystyrene at shear rates up to several hundred have been obtained using a Lodge Stressmeter [47] and a sliding plate rheometer (SPR), and polystyrene data obtained using both techniques are compared in Fig. 2.21 [48]. The data were found to be in good agreement with an empirical relationship proposed by Laun [49], shown below as Eq. (2.31)

$$\Psi_1(\dot{\gamma}) = 2\frac{G'}{\omega^2}\left[1 + \left(\frac{G'}{G''}\right)^2\right]^{0.7}. \tag{2.31}$$

The dimensionless quantity $N_1(\dot{\gamma})/\sigma(\dot{\gamma})$ is called the *stress ratio* SR and indicates the relative importance of orientation or stored elastic energy at a given shear rate. The ratio $N_1(\dot{\gamma})/2\sigma(\dot{\gamma})$, i.e., SR/2, is often called the *recoverable shear*. However, it is only equal to the actual strain recovered after sudden release of the shear stress during steady shear, at low shear rates.

References

1. Bird RB, Armstrong RC, Hassager O (1987) Dynamics of Polymeric Liquids, vol 1. Wiley, New York
2. Meissner J (1971) Deformationsverhalten der Kunststoffe im flüssigen und im festen Zustand. Kunststoffe 61:576–582
3. Stratton RA (1966) The dependence of non-Newtonian viscosity on molecular weight for "Monodisperse" polystyrene. J Colloid Interface Sci 22:517–530
4. Cross MM (1965) Rheology of non-Newtonian fluids: a new flow equation for pseudoplastic systems. J Coll Sci 20:417–437
5. Carreau PJ (1972) Rheological equations from molecular network theories. Trans Soc Rheol1 6:99–127
6. Hieber CA, Chiang HH (1992) Shear-rate-dependence modeling of polymer melt viscosity. Polym Eng Sci 14:931–938
7. Yasuda KY, Armstrong RC, Cohen RE (1981) Shear flow properties of concentrated solutions of linear and star-branched polystyrenes. Rheol Acta 20:163–178
8. Elberli B, Shaw MT (1978) Time constants from shear viscosity data. J Rheol 22:561–570

9. Plumley TA, Lai S, Betso SR, Knight GW (1994) Rheological modeling of Insite technology polymers. SPE ANTEC Tech Papers 40:1221–1224
10. Wang J (2010) Double cross model—A novel way to model viscosity curves, Society of Rheology. 82nd annual meeting, Santa Fe, NM
11. Cox WP, Merz EH (1958) Correlation of dynamic and steady flow viscosities. J Polym Sci 28:619–621
12. Utracki LA, Gendron R (1984) Pressure oscillation during extrusion of polyethylenes. J Rheol 28:601–623
13. Venkatraman S, Okano M, Nixon AA (1990) A comparison of torsional and capillary rheometry for polymer melts: the Cox-Merz rule revisited. Polym Eng Sci 30:308–313
14. Park HE, Dealy JM (2006) Effect of pressure and supercritical CO2 on the viscosity of Polyethylene. Macromolecules 39:5438–5452
15. Park HE, Dealy JM, Münstedt H (2006) Influence of long-chain branching on time-pressure and time-temperature shift factors for polystyrene and polyethylene. Rheol Acta 46:153–159
16. Berry GC, Fox TG (1968) The viscosity of polymers and their concentrated solutions. Adv Polym Sci 5:261–357
17. Bartels CR, Crist B, Fetters LJ, Graessley WW (1986) Self-diffusion in branched polymer melts. Macromol 19:785–793
18. Struglinski MJ, Graessley WW (1985) Effects of polydispersity on the linear viscoelastic properties of entangled polymers 1: experimental observations for binary mixtures of linear polybutadiene. Macromol 18:2630–2643
19. Kumar R, Khanna YP (1989) SPE Tech. Papers 35, 1675
20. Shroff AR, Mavridis H (1995) New measures of polydispersity from rheological data on polymer melts. J Appl Polym Sci 57:1605–1626
21. Fuchs K, Chr Friedrich, Weese J (1996) Viscoelastic properties of narrow-distribution poly(methylmethacrylates). Macromol 29:5893–5901
22. Huang CL, Chen YC, Hsiao TJ, Tsai JC, Wang C (2011) Effect of tacticity on viscoelastic properties of poplystyrene. Macromol 44:6155–6161
23. Wood-Adams P, Dealy JM, deGroot AW, Redwine OD (2000) Rheological properties of metallocene polyethylenes. Macromol 33:7489–7499
24. Wood-Adams P, Costeux S (2001) Thermorheological behavior of polyethylene: effects of microstructure and long chain branching. Macromol 34:6281–6290
25. Garcia-Franco CA, Harrington BA, Lohse DJ (2006) Effect of short-chain branching on the rheology of polyolefins. Macromol 39:2710–2717
26. Dealy JM, Larson RG (2006) Structure and rheology of molten polymers. Hanser Publishers, Munich
27. Pearson DS, Helfand E (1984) Viscoelastic properties of star-shaped polymers. Macromol 17:888–895
28. Kraus G, Gruver JT (1965) Rheological properties of multichain polybutadienes. J Polym Sci A 3:105–122
29. Graessley WW, Roovers J (1979) Melt Rheology of four-arm and six-arm star polystyrenes. Macromol 12:959–965
30. Gell CB, Graessley WW, Efstratiadis V, Pitsikalis M, Kadjichristidis N (1997) Viscoelasticity and self-diffusion in melts of entangled asymmetric star polymers. J Polym Sci, Part B: Polym Phys 35:1943–1954
31. Stevens JC (1994) INSITE^{TM} catalyst structure/activity relationships for olefin polymerization. Stud Surf Sci Catal 89:277–284; Constrained geometry and other single site metallocene polyolefin catalysts: A revolution in olefin polymerization. *Ibid*. (1996) 101:11–20
32. Lai SY, Wilson JR, Knight JR, Stevens JC (1993) Elastic substantially linear olefin polymers. US Patent 5(380):810
33. Soares JBP, Hamielec AE (1996) Bivariate chain length and long chain branching distribution for copolymerization of olefins and polyolefin chains containing terminal double-bonds. Macromol Theory Simul 5:547–572

34. Soares JBP, Hamielec AE (1997) The chemical composition component of the distribution of chain length and long chain branching for copolymerization of olefins and polyolefin chains containing terminal double bonds. Macromol Theory Simul 6:591–596
35. Read DJ, McLeish TCB (2001) Molecular rheology and statistics of long chain branched metallocene-catalyzed polyolefins. Macromol 34:1928–1945
36. Costeux S, Wood-Adams P, Beigzadeh D (2002) Molecular structure of metallocene-catalyzed polyethylene: rheologically relevant representation of branching architecture in single catalyst and blended systems. Macromol 35:2514–2528
37. Soares JBP (2004) Polyolefins with long chain branches made with single-site coordination catalysts: a review of mathematical modeling techniques for polymer microstructure. Macromol Mater Eng 289:70–87
38. Wood-Adams PM, Dealy JM (2000) Using rheological data to determine the branching level in metallocene polyethylenes. Macromol 33:7481–7488
39. Robertson CG, García-Franco CA, Srinivas S (2004) Extent of branching from linear viscoelasticity of long-chain branched polymers. J Polym Sci, Part B: Polym Phys 42:1671–1684
40. Auhl D, Stange J, Münstedt H, Krause B, Voigt D, Lederer A, Lappan U, Lunkwitz K (2004) Long-chain branched polypropylenes by electron beam irradiation and their rheological properties. Macromol 37:9465–9472
41. Gabriel C, Münstedt H (2003) Strain hardening of various polyolefins in uniaxial elongational flow. J Rheol 47:619–630
42. Gabriel C, Kokko E, Löfgren B, Seppälä J, Münstedt H (2003) Analytical and rheological characterization of long-chain branched metallocene-catalyzed ethylene homopolymers. Polymer 43:6383–6390
43. Wang J, Mangnus M, Yau W, deGroot W, Karjala T, Demirors M (2008) Structure-property relationships of LDPE. SPE ANTEC Tech Papers, pp 878–881
44. Gabriel C, Lilge D (2006) Molecular mass dependence of the zero shear-rate viscosity of LDPE melts: evidence of an exponential behavior. Rheol Acta 45:995–1002
45. Schweizer T, van Meerveld J, Öttinger HC (2004) Nonlinear shear rheology of polystyrene melt with narrow molecular weight distribution—experiment and theory. J Rheol 48:1345–1363
46. Lee CS, Magda JJ, DeVries KL, Mays JW (1992) Measurements of the second normal stress difference for star polymers with highly entangled branches. Macromol 25:4744–4750
47. Lodge AS (1996) On-line measurement of elasticity and viscosity in flowing polymeric liquids. Rheol Acta 35:110–116
48. Xu J, Costeux S, Dealy JM, De Decker MN (2007) Use of a sliding plate rheometer to measure the first normal stress difference at high shear rates. Rheol Acta 46:815–824
49. Laun HM (1986) Prediction of elastic strains of polymers melts in shear and elongation. J Rheol 30:459–501

http://www.springer.com/978-94-007-6394-4

Melt Rheology and its Applications in the Plastics Industry

Dealy, J.M.; Wang, J.

2013, XVI, 282 p., Hardcover
ISBN: 978-94-007-6394-4